Journal of The Electrochemical Society, **154** (10) J302-J305 (2007)
0013-4651/2007/154(10)/J302/4/$20.00 © The Electrochemical Society

High-Luminance Top-Emitting Organic Light-Emitting Diodes Using Cs/Al/Au as the Semitransparent Multimetal Cathode

J. T. Lim,[a] C. H. Jeong,[a] J. H. Lee,[a] G. Y. Yeom,[a,z] E.-C. Shin,[b] E. H. Lee,[b] and T. W. Kim[b]

[a]*School of Advanced Materials Science and Engineering, Sungkyunkwan University, Suwon 440-746, Korea*
[b]*Department of Information Display Engineering, Hongik University, Seoul 121-791, Korea*

Top-emitting organic light-emitting diodes (TEOLEDs) using an ultrathin cesium (Cs) layer capped with a semitransparent Al/Au layer as an effective, electron-injecting cathode were fabricated by vacuum evaporation. The optical properties of Cs (20 nm)/Al (20 nm)/Au (20 nm) at a wavelength of 520 nm exhibited a transmittance of 59% and a reflectance of 14%. The Cs/Al/Au cathode showed lower power consumption and higher luminance at the same forward bias voltage than the Cs/Al/Ag cathode. Using a tris(8-quinolinolato)aluminum(III) (Alq_3) layer as the emissive material, a TEOLED based on the Cs/Al/Au cathode showed a maximum luminance of 66,200 cd/m^2 at 9.8 V. An external quantum efficiency and the power efficiency of 1.6% and 2.1 lm/W, respectively, at a luminance of 1000 cd/m^2 (corresponding to a bias voltage of 6.2 V) was obtained. The good driving performance of this TEOLED was attributed to the excellent optical properties such as high transmittance and efficient-electron injection from the Cs/Al/Au to the adjoining organic layer.
© 2007 The Electrochemical Society. [DOI: 10.1149/1.2759842] All rights reserved.

Manuscript submitted July 13, 2006; revised manuscript received May 25, 2007. Available electronically August 8, 2007.

Organic light-emitting diode (OLED) displays are being actively developed as one of the best flat panel display (FPD) technologies suitable for information-display applications in the next generation of displays. Developing top-emitting (TE) OLED structures coupled with a low-temperature polysilicon (LTPS) thin-film transistor (TFT) backplane is one of the most important key-element techniques in active-matrix (AM) OLED displays. A TEOLED can provide not only a higher aperture ratio than the general bottom-emitting (BE) diodes, but can also display higher image quality on account of its geometrical merit allowing a high pixel resolution.[1,2] In addition, the TEOLED structure can more easily allow the stacking of either a color filter (CF) or a color change medium (CCM) onto the top of the TEOLEDs, which can allow more choices of substrates and control the color purity of the light irradiated more easily by modifying the microcavity structure than BEOLEDs.

In TEOLEDs, semitransparent top cathodes play an important role in achieving good device performance. Many attempts have been made to develop proper top cathodes.[2-12] Particular attention has been focused on the development of cathode systems such as semitransparent conducting buffer layers (STCBL)/transparent conducting oxides (TCOs) [e.g., Ag-doped Mg/tin-doped indium oxide (ITO)[7,8] and Ca/ITO[9]], multimetal cathode systems [e.g., Ca/Ag,[10] Ca/Mg,[11] and LiF/Al/Ag [12]] and metal-free cathode systems [e.g., copper phthalocyanine (CuPc)/ITO,[3] Li-doped 2,9-dimethyl-4,7-diphenyl-l,10-phenanthroline (BCP)/ITP,[2] and Li-doped 4,7-diphenyl-l,10-phenanthroline (Bphen)/ITO[4]]. Here, STCBL have been used to prevent physical-chemical damage to the organic layers occurring during sputtering deposition of the transparent conducting oxides (TCOs) such as ITO in TEOLEDs. If a TEOLED using a TCO layer does not have an STCBL, the TCO sputtering process can cause serious damage to the organic layers. In addition, the damaged organic layers in the TEOLED can cause many problems such as high leakage current, low luminous efficiency, short lifetime, etc. Therefore, it would be beneficial if the cathode system of the TEOLED could be fabricated by the vacuum evaporation of multimetals.

Among the various metals, semitransparent Au might be a good candidate for the cathode composing the TEOLED owing to its low resistance, high transmittance, and high stability. However, the work function (Φ) of Au (5.1 eV)[13] is too large for efficient electron injection into an adjoining layer such as Alq_3 lowest occupied molecular orbital (LUMO level: 3.1 eV) in the OLED. Therefore, an electron-injecting layer such as Cs (Φ: 2.14 eV)[13] is essential for enhancing the electron injection. In addition, the multimetal cathode system should satisfy two conflicting requirements simultaneously, i.e., high electrical conductivity and high optical transmittance, to maintain the characteristics of an intrinsic top emission.

This paper reports a TEOLED, which has a structure consisting of glass/Ag (100 nm)/ITO (125 nm)/2-TNATA (30 nm)/NPB (15 nm)/Alq_3 (55 nm)/Cs (x nm)/Al (2.0 nm)/Au (20 nm)/Alq_3 (52 nm). As a reference, the TEOLED with a multimetal cathode consisting of Cs/Al/Ag was also fabricated, and its material and device characteristics were compared with those of Cs/Al/Au. In addition, the effect of the Cs thickness as an electron-injecting layer on the TEOLED device properties were investigated by varying the thickness of Cs in the Cs/Al/Au layer.

Experimental

All the organic layers and multimetal layer cathodes composing TEOLEDs were deposited by thermal evaporation. The silver composing the multilayer anode was deposited by electron beam evaporation. The ITO in the multilayer anode was deposited by conventional dc sputtering followed by heat treatment. The inset in Fig. 1a shows a schematic diagram of the device structure for devices 1–3 consisting of glass/Ag (100 nm)/ITO (125 nm, about 20–30 Ω/□)/2-TNATA (30 nm)/NPB (15 nm)/Alq_3 (55 nm)/Cs (x nm)/Al (2 nm)/Au (20 nm)/Alq_3 (52 nm) (x = 2.5, 2.0, and 0.5 nm). Device 4 has the same structure as device 3, except that Ag was used in the multimetal layer cathode instead of Au. Here, Cs was deposited using a standard SAES getter source. The emissive active area of the devices was 1.4 × 1.4 mm. Tris(8-quinolinolato)aluminum(III) (Alq_3, refractive index: 1.7 [14]), which is a transparent dielectric index-matching layer that can enhance optical transmission, was used as the top capping layer of the TEOLED.

The reflectance spectrum and the transmittance spectrum of the electrodes were measured using a UV-vis-NIR spectrophotometer in which an external DRA (Cary 5000 UV/vis/NIR, Varian Inc.) was attached and a UV spectrophotometer (UV S-2100, Scinco Inc.), respectively. The resistivity was measured using a four-point probe (CMT-Series, Chang Min Co. Ltd.). Current-voltage-luminance characteristics were measured using a source-measure unit (2400, Keithley Instrument Inc.), and the emission intensity of the OLED devices was measured by the photocurrent induced on the silicon photodiodes using a picoammeter (485, Keithley Instrument Inc.). The luminance and external quantum efficiency were calculated

[z] E-mail: gyyeom@skku.edu

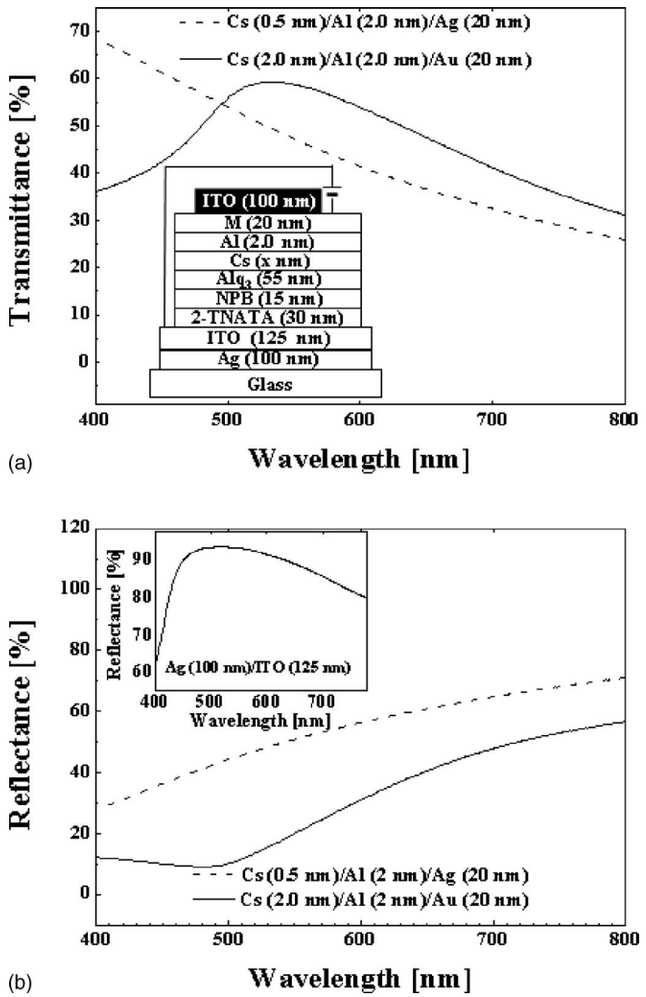

Figure 1. (a) Transmittance spectra of both the Cs (2.0 nm)/Al (2.0 nm)/Au (20 nm) (solid line) and the Cs (0.5 nm)/Al (2.0 nm)/Ag (20 nm) cathode (dash line). The inset shows the schematic device structure of the TEOLEDs consisting of glass/Ag (100 nm)/ITO (125 nm)/2-TNATA (30 nm)/NPB (15 nm)/Alq_3 (55 nm)/Cs (x nm)/Al (2 nm)/M (20 nm)/Alq_3 (52 nm) (M: Au or Ag). (b) Reflectance spectra of both the Cs (2.0 nm)/Al (2.0 nm)/Au (20 nm) (solid line) and the Cs (0.5 nm)/Al (2.0 nm)/Ag (20 nm) cathode. The inset is the reflectance spectrum of the Ag (100 nm)/ITO (125 nm) anode.

from responsivity (silicon photodiode) and photopic efficiency (photopic response curve) compensated by the electroluminescence spectrum measured using optical emission spectroscopy (PCM-420, SC Tech. Inc.).

Results and Discussion

The inset of Fig. 1a shows the device configuration of the TEOLEDs. The device structure consisted of glass/Ag (100 nm)/ITO (125 nm)/2-TNATA (3 nm)/NPB (15 nm)/Alq_3 (55 nm)/Cs (x nm)/Al (2 nm)/M (20 nm)/Alq_3 (52 nm). Here, M is either Au for devices 1–3 or Ag for device 4. The thickness of Cs in devices 1, 2, 3, and 4 was 2.5, 2.0, 0.5, and 0.5 nm, respectively. In the case of the devices with a multimetal layer cathode of Cs (x nm)/Al (2.0 nm)/Ag (20 nm), when the Cs thickness was changed from 0 and 2.0 nm, the device (device 4) with the Cs thickness of 0.5 nm showed the highest driving performance (not shown). In the above TEOLED structure, 4,4′,4″-tris[2-naphthylphenyl-1-phenylamino]triphenylamine (2-TNATA) was used as the hole-injecting layer (HIL), 4,4′-bis[*N*-(l-napthyl)-*N*-phenylamino]-biphenyl (NPB) was used as the hole-transporting layer (HTL), and Alq_3 was used as both the emissive layer and an electron-transporting layer (ETL).

To achieve a good driving performance, it is essential to obtain ohmic interfaces between the adjoining organic layer and the charge-injecting contacts of the electrodes. In this TEOLED structure, ohmic contact to a hole injection layer can be achieved when the ionization potential (IP) of 2-TNATA is the same as or lower than the work function of the adjoining anode. In addition, ohmic contact to an electron injection layer can be realized when the electron affinity (EA) of Alq_3 is the same as or higher than the work function of the adjoining cathode. In the TEOLEDs, the energy barrier (ΔB) for hole injection between ITO (Φ: 4.7 eV)[3] and 2-TNATA (IP: 5.1 eV)[15] is 0.4 eV. However, ΔB for electron injection between Al (Φ: 4.3 eV)/Au composing the multilayer cathode and Alq_3 (EA: 3.1 eV)[16] is approximately 1.2 eV. Therefore, ΔB for the electron injection is higher than that for hole injection. This nonohmic characteristic of the above cathode/Alq_3 structure was demonstrated through the current-voltage curves reported by Parthasarathy et al.[17] Even though the ohmic contacts between the cathode and an adjoining organic layer cannot be well formed, the injection of an electron carrier into Alq_3 is expected to be improved by introducing a low work function material between Alq_3 and Al/Au to reduce the electron injection barrier, such as Cs. In addition, the use of Cs with a low Φ of 2.14 eV between the adjoining cathode and Alq_3 is expected to show good device performance through efficient electron injection.

Meanwhile, in the Cs/Al/Au cathode, Al was used as the glue layer between the Cs and Au, while the Au layer was used as a protective layer to prevent oxidation of both Cs and Al from both atmospheric moisture and oxygen in air. An ultrathin layer of Au has a relatively low optical reflectance, high transmittance, and similar conductivity compared with Ag. Meanwhile, as reported by Hung et al., Alq_3 (refractive index: 1.7 [14]) was used as the dielectric refractive index-matching layer to enhance optical transmission with air (refractive index: 1.0) and as a semipassivation layer to protect the device.

The optical properties of the TEOLED structure with two reflective mirrors strongly depend on the microcavity effect.[18] Recently, Riel et al. suggested an excellent model for enhancing the enhancement of the light outcoupling to the top position in the TEOLED structure.[11] The optical model in their TEOLED contains partial reflections at the interfaces between the electrodes. As a result, interference effects can occur, which are based on the equivalence between the wide-angle interference effects from an electrical dipole transition and the multiple-beam interference effects from an electrical dipole antenna. From these models, they demonstrated that light emission is not the maximum at the highest transmittance of the cathode, but that rather it is determined by interplay between the different interference effects. Therefore, enhanced light outcoupling efficiency at the top position of the TEOLED structure can be obtained through the highest transmittance related to the interference effects.

In this TEOLED structure, in order to obtain a high aperture ratio, Ag/ITO was used as a highly reflective anode with a low resistance, and Cs/Al/Au was used as a highly transmissive cathode with a low resistance. Figure 1a shows the transmittance spectra of both Cs (2.0 nm)/Al (2.0 nm)/Au (20 nm) and Cs (0.5 nm)/Al (2.0 nm)/Ag (20 nm) over the visible range. In addition, Fig. 1b shows the reflectance spectra of these multimetal layer cathodes. The transmittance of Cs (2.0 nm)/Al (2.0 nm)/Au (20 nm) at a wavelength of 520 nm (±1 nm) and Cs (0.5 nm)/Al (2.0 nm)/Ag (20 nm) at a wavelength of 515 nm was 58.8 and 51.8%, respectively, whereas the reflectance of these multimetal layer cathodes was 13.5% at 520 nm (±1 nm) and 46.4% at 515 nm. Therefore, the multimetal cathode consisting of Cs (2.0 nm)/Al (2.0 nm)/Au (20 nm) showed higher transmittance and lower reflectance than the multimetal cathode

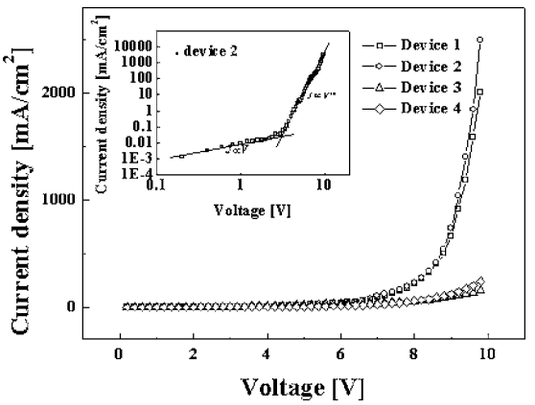

Figure 2. Current density as a function of the voltage for devices 1 (square), 2 (circle), 3 (triangle), and 4 (diamond). The inset shows log J vs log V plot for device 2.

consisting of Cs (0.5 nm)/Al (2.0 nm)/Ag (20 nm), even though the Cs thickness was higher. The wavelength of 520 nm (±1 nm) and 515 nm is the maximum peak of the EL spectrum for devices 1–3 and device 4, respectively. As a result, the multimetal layer cathode of Cs (2.0 nm)/Al (2.0 nm)/Au (20 nm) in TEOLEDs is expected to have a higher aperture ratio than that of Cs/Al/Ag. The inset in Fig. 1b shows the reflectance spectrum of the multimetal layer anode consisting of Ag (100 nm)/ITO (125 nm) as a function of the wavelength over the visible range. The reflectance at the wavelength of 520 nm was 94%.

As is well known, when light propagates through a metal it can penetrate a small distance inside the metal before it is reflected. This characteristic length depends on the wavelength of the incident light, and is referred as the skin depth (δ). The high reflectivity of Cs (0.5 nm)/Al (2.0 nm)/Ag (20 nm) is mainly attributed to the silver thickness. The δ of silver can be expressed as follows: $\delta = \lambda 4\pi n_i$ (λ: wavelength of light, n_i: imaginary component of the index of refraction). δ is approximately 14 nm when $\lambda = 5 \times 10^{-7}$ m and $n_i = 2.88$.[19] Therefore, Cs (0.5 nm)/Al (2.0 nm)/Ag (20 nm) exhibits high reflectance because the 20 nm thick silver composing Cs (0.5 nm)/Al (2.0 nm)/Ag (20 nm) was thicker than the skin depth, as shown in Fig. 1b. However, in the case of gold, δ is approximately 22 nm when λ and n_i are 5×10^{-7} m and 1.84, respectively.[20] Therefore, a 20 nm thick gold layer in the Cs (2.0 nm)/Al (2.0 nm)/Au (20 nm) cathode is within the skin depth while the 20 nm thick silver layer is outside of the skin depth. The improved optical properties of Cs/Al/Au, as shown in Fig. 1a and b, are believed to be the result of differences in the skin depth. Meanwhile, the resistivity of Cs (0.5 nm)/Al (2 nm)/Au (20 nm) and Cs (2.0 nm)/Al (2.0 nm/Ag were similar as 9.1×10^{-6} and 8.0×10^{-6} Ω cm, respectively. Therefore, Cs (2.0 nm)/Al (2.0 nm)/Au (20 nm) are expected to be more desirable as the multimetal cathode for TEOLED than Cs (0.5 nm)/Al (2.0 nm)/Ag (20 nm). The resistivity was 4.0×10^{-6} Ω cm in the case of the multilayer anode consisting of Ag (100 nm)/ITO (125 nm).

Figure 2 shows the current density as a function of the forward bias voltage for devices 1, 2, 3, and 4. Table I summarizes the results of the current density-voltage-luminance characteristics for devices 1, 2, 3, and 4. At a luminance of approximately 1000 cd/m^2 (L_{1000}), the current densities of devices 1, 2, and 3 with the Cs (x nm)/Al/Au cathode were 47.6 (6.2 V), 34.4 (6.2 V), and 57.8 mA/cm^2 (8.0 V), respectively. When the thickness of Cs was varied between 0.5 and 2.5 nm, as shown in Fig. 2, the current density-voltage curves of the fabricated TEOLEDs showed the lowest power consumption at a thickness of 2.0 nm (device 2). Table I also shows the luminous efficiencies of devices 1–4 at L_{1000}. Device 2, with a 2.0 nm thick Cs layer, is expected to have the highest power efficiency (η_{PE}) at L_{1000} because the power (W) is inversely proportional to η_{PE} at the same pixel area according to the general equation, $\eta_{PE} = \pi L/JV$ (J: current density, V = bias voltage).

The inset in Fig. 2 shows the current density (J) as a function of the forward bias voltage (V) in a logarithmic scale for device 2. As shown in the figure, the device operation can be divided into two regions, above and below the turn voltage (V_T) of 2.8 V. Above V_T, the current is trapped-charge limited and follows the power law, $I \propto V^{(m+1)}$. In device 2, m is approximately 9, while it is in the range of 6–8 for devices 1, 3, and 4.

The inset of Fig. 3a shows the EL spectrum of devices 1, 2, 3, and 4 measured at the normal viewing angle and at L_{1000}. As shown in the inset of Fig. 3a, the maximum peak of the EL spectrum for devices 1, 2, 3 was found at wavelengths of 520, 520, and 521 nm, respectively. The full width at a half-maximum (fwhm) of devices 1, 2, and 3 was similar at 61 nm. The EL maximum peak of device 4 occurred at 515 nm and its fwhm was 59 nm. The wavelength of the EL spectra of each device can be tuned by adjusting the macrocavity effects,[18] which are controlled by changing the thickness of the ITO layer in the multilayer anode or the total thickness of the organic layers.

The luminance (L_{max}) at a voltage of 9.8 V for devices 1, 2, and 3 was 49,000, 66,200, and 4050 cd/m$_2$, respectively, as shown in Table I and Fig 3a. Here, the voltage (9.8 V) at the maximum luminance of device 2 was used as the reference voltage to compare the luminance of the other devices because the power consumption of device 2 was the lowest among the devices with Cs/Al/Au, as mentioned above. Among devices 1, 2, and 3, device 2 with a 2.0 nm thick Cs showed the highest luminance, possibly from the efficient electron injection due to the low-energy barrier between Cs and the adjoining Alq_3. Device 4 showed lower luminance characteristic than devices 1 and 2. In particular, at a forward bias voltage of 9.8 V, device 2 showed approximately 5.5 times higher luminance than device 4.

As shown in devices 1, 2, and 3 in Fig. 3a, the luminance of these devices increased with increasing Cs thickness from 0.5 to 2.0 nm. However, the luminance is decreased with further increases in Cs thickness to 2.5 nm. The lower luminescence at the lower Cs thickness appears to be related to the complete consumption of the

Table I. Current density-voltage-luminance characteristics of devices 1–4.

Devices	STCPL (nm)	η_{ext} (%)	η_{PE} (lm/W)	V_{1000} (V)	V_T (V)	L (cd/m^2)
Device 1	Cs (2.5)/Al (2.0)/Au (20)	1.5	2.1	6.2	2.8	49,000
Device 2	Cs (2.0)/Al (2.0)/Au (20)	1.6	2.1	6.2	2.8	66,200
Device 3	Cs (0.5)/Al (2.0)/Au (20)	1.1	1.4	8.0	3.0	4,050
Device 4	Cs (0.5)/Al (2.0)/Ag (20)	1.6	2.0	6.6	2.8	11,900

η_{ext}, η_{PE}, and V_{1000} were measured at 1000 cd/m^2, respectively. V_T and L are a turn-on voltage at the luminance of 0.1 cd/m^2 and a luminance at the forward bias voltage of 9.8 V, respectively.

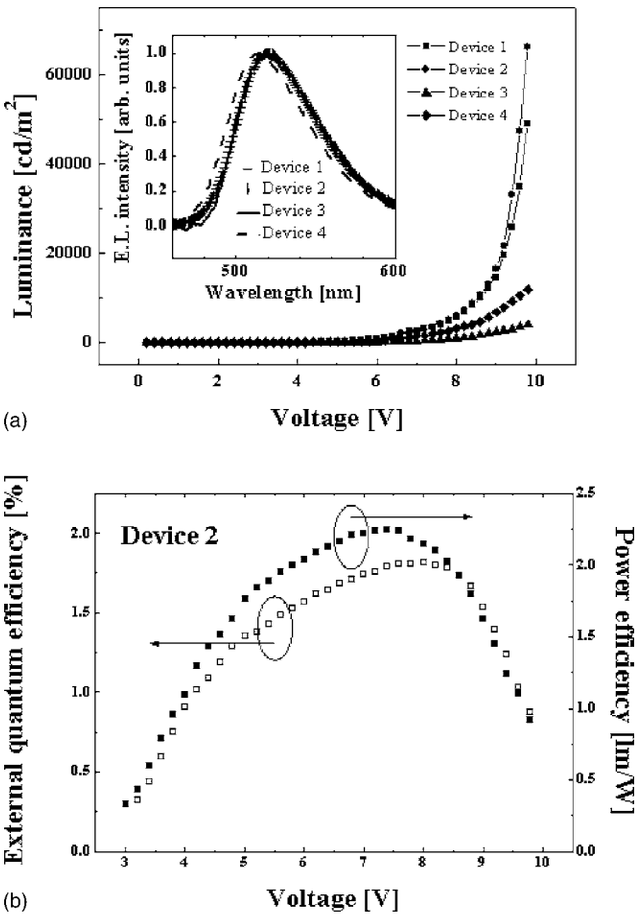

Figure 3. (a) Luminance-voltage characteristic of devices 1 (square), 2 (circle), 3 (triangle), and 4 (diamond). The inset shows electroluminescent spectrum at a luminance of 1000 cd/m^2 for device 1 [bar (–) symbol] device 2 [bar (|) symbol], device 3 (solid line), and device 4 (dash line), respectively. (b) The external quantum efficiency-voltage (open square) and power efficiency-voltage characteristic (closed square) of device 2.

deposited thin Cs by Alq_3 as a result of the reaction and diffusion. The decrease in luminescence at a Cs thickness >2.0 nm appears to be partially related to the decrease in optical transmittance with increasing Cs thickness, even though the precise reason for the decrease in luminance is unclear and requires further investigation. From the above results, it is believed that the optimal device characteristics can be obtained when a Cs layer remains between Alq_3 and Au without blocking light transmission.

As shown in Table I, the external quantum efficiencies (η_{ext}) at L_{1000} of devices 1, 2, and 3 were 1.5, 1.6, and 1.1%, respectively. The η_{PE} for devices 1, 2, and 3 were 2.1, 2.1, and 1.4 lm/W, respectively. Therefore, device 2 showed not only the highest η_{PE} but also the highest η_{ext}. Figure 3b shows the η_{ext} and η_{PE} of device 2 as a function of forward bias voltage. The luminous efficiencies in the case of device 4 at L_{1000} showed an η_{ext} and η_{PE} of 1.6 lm/W and 2.0%, respectively. Therefore, in view of both the luminance and the luminous efficiency, device 2 with a Cs/Al/Au cathode showed higher light output characteristics than that with the Cs/Al/Ag cathode.

Conclusion

A conventional TEOLED using a Cs/Al/Au cathode was fabricated by sequential deposition with a structure consisting of glass/Ag (100 nm)/ITO (125 nm)/2-TNATA (30 nm)/NPB (15 nm)/Alq_3 (55 nm)/Cs (x nm)/Al (2 nm)/Au (20 nm)/Alq_3 (52 nm). A multimetal layer cathode consisting of Cs (2.0 nm)/Al (2.0 nm)/Au (20 nm) showed a transmittance of 59% and a reflectance of 14%, respectively, at a wavelength of 520 nm. When the Cs thickness in the TEOLED was changed, the TEOLED with the 2.0 nm thick Cs showed the best driving performance in view of both the luminous efficiency and luminance. The light output of this TEOLED exhibited an L_{max} of 66,200 cd/m^2 at a forward bias voltage of 9.8 V. In addition, its η_{ext} and η_{PE} at L_{1000} (about 6.2 V) were 1.6% and 2.1 lm/W, respectively. This driving performance obtained for the TEOLED with Cs (2.0 nm)/Al (2.0 nm)/Au (20 nm) was estimated to be the result of the small energy barrier, which is involved with the efficient electron injection at the interface between Cs with the low work function and Alq_3. The TEOLED with Cs (2.0 nm)/Al (2.0 nm)/Au (20 nm) showed approximately 5.5 times higher brightness at 9.8 V than the TEOLED of the same structure with Cs (0.5 nm)/Al (2.0 nm)/Ag (20 nm). In particular, devices with a multimetal layer cathode of Cs (2.0 nm)/Al (2.0 nm)/Au (20 nm) showed good driving performance at the high current of the trapped-charge limit range.

Acknowledgments

This work was supported by a National Research Laboratory Program (NRL) of the Ministry of Science & Technology and by Sungkyunkwan University (2005).

Sungkyunkwan University assisted in meeting the publication costs of this article.

References

1. G. Gu, G. Parthasarathy, P. E. Burrows, P. Tian, I. G. Hill, A. Khan, and S. R. Forrest, *J. Appl. Phys.*, **86**, 4076 (1999).
2. G. Parthasarathy, C. Adachi, P. E. Burrows, and S. R. Forrest, *Appl. Phys. Lett.*, **76**, 2128 (2000).
3. G. Parthasarathy, P. E. Burrows, V. Khalfin, V. G. Kozlov, and S. R. Forrest, *Appl. Phys. Lett.*, **72**, 2138 (1998).
4. H. Kanno, Y. Sun, and S. R. Forrest, *Appl. Phys. Lett.*, **86**, 263502 (2005).
5. S. L. Lai, M. K. Fung, S. N. Bao, S. W. Tong, M. Y. Chan, C. S. Lee, and S. T. Lee *Chem. Phys. Lett.*, **367**, 753 (2003).
6. G. He, O. Schneider, D. Qin, X. Zhou, M. Pfeiffer, and K. Leo, *J. Appl. Phys.*, **95**, 5773 (2004).
7. V. Bulovic, G. Gu, D. E. Burrows, M. E. Thompson, and S. R. Forrest, *Nature (London)*, **380**, 29 (1996).
8. G. Gu, V. Bulovic, P. E. Burrows, S. R. Forrest, and M. E. Thompson, *Appl. Phys. Lett.*, **68**, 2606 (1996).
9. M.-H. Lu, M. S. Weaver, T. X. Zhou, M. Rothman, R. C. Kwong, M. Hack, and J. J. Brown, *Appl. Phys. Lett.*, **81**, 3921 (2002).
10. R. B. Pode, C. J. Lee, D. G. Moon, and J. I. Han, *Appl. Phys. Lett.*, **84**, 4614 (2004).
11. H. Reil, S. Karg, T. Beierlein, and W. Reiß, *J. Appl. Phys.*, **94**, 5290 (2003).
12. C.-W. Chen, P. Y. Hsieh, H. H. Chaing, C. L. Lin, H.-M. Wu, and C.-C. Wu, *Appl. Phys. Lett.*, **83**, 5127 (2003).
13. W. Benenson, J. W. Harris, H. Stocker, and H. Lutz, *Handbook of Physics*, p. 1082 Springer-Verlag, New York (2002).
14. L. S. Hung, M. Tang, M. G. Mason, P. Raychaudhuri, and J. Madathil, *Appl. Phys. Lett.*, **78**, 544 (2001).
15. K. Okumoto and Y. Shirota, *J. Lumin.*, **87–89**, 1171 (2000).
16. M. A. Baldo and S. R. Forrest, *Phys. Rev. B*, **62**, 10958 (2000).
17. G. Parthasarathy, C. Shen, A. Kahn, and S. R. Forrest, *J. Appl. Phys.*, **89**, 4986 (2001).
18. P. E. Burrows, Z. Shen, V. Bulovic, D. Z. McCarty, S. R. Forrest, J. A. Cronin, and M. E. Thompson, *J. Appl. Phys.*, **79**, 7991 (1996).
19. M. Scalora, M. J. Bloemer, A. S. Pehtel, J. P. Dowling, C. M. Bowden, and A. S. Manka, *J. Appl. Phys.*, **83**, 2377 (1998).
20. *Handbook of Optical Constants of Solids*, E. D. Palik, Editor, Academic, New York (1985).